Adaptive Tracking Control with Uncertainty-aware and State-dependent Feedback Action Blending for Robot Manipulators

Wu, Xuwei and Kirner, Annika and Garofalo, Gianluca and Ott, Christian and Kotyczka, Paul and Dietrich, Alexander

Adaptive Tracking Control with Uncertainty-aware and State-dependent Feedback Action Blending for Robot Manipulators

Xuwei Wu, Annika Kirner, Gianluca Garofalo, Christian Ott, Paul Kotyczka, and Alexander Dietrich

***Abstract*—Adaptive control can significantly improve tracking performance of robot manipulators subject to modeling errors in dynamics. In this letter, we propose a new framework combining the composite adaptive controller using a natural adaptation law and an extension of the adaptive variance algorithm (AVA) for controller blending. The proposed approach not only automatically adjusts the feedback action to reduce the risk of violating actuator constraints but also anticipates substantial modeling errors by means of an uncertainty measure, thus preventing severe performance deterioration. A formal stability analysis of the closed-loop system is conducted. The control scheme is experimentally validated and directly compared with baseline methods on a torque-controlled KUKA LWR IV+.**

***Index Terms*—Adaptive control, motion control, automatic feedback action blending, uncertainty measure.**

I. Introduction

AUTONOMOUSLY and appropriately adapting the behavior to internal parameter variations and unforeseeable external contacts is an essential feature for a robot that needs to perform versatile manipulation in unknown and unstructured environments. To attain high tracking accuracy under model uncertainties at run-time, e.g., due to manipulation of an unknown object, it is common to use model-based adaptive control, which performs online parameter adaptation driven by tracking errors [1], prediction errors [2], or both error sources in a composite manner [3]. Recently, Lee *et al.* [4] proposed a natural adaptation law that guarantees the physical consistency [5], [6] of the estimated inertial parameters, with additional advantages of improved transient performance and less laborious gain selection; a recent application can be found in [7]. However, these adaptive control schemes only adapt the feedforward term but do not adjust the feedback term according to model uncertainties. In fact, a high-gain feedback action is particularly needed to compensate for substantial modeling errors during the initial phase of parameter adaptation. The saturation-based robust controller [8] can effectively handle this issue but requires an *a priori* uncertainty bound and only achieves ultimate boundedness of the tracking error. For nonlinear systems transformable into the *parametric strict feedback* form, backstepping adaptive control [9] can improve the transient performance under large initial estimation errors.

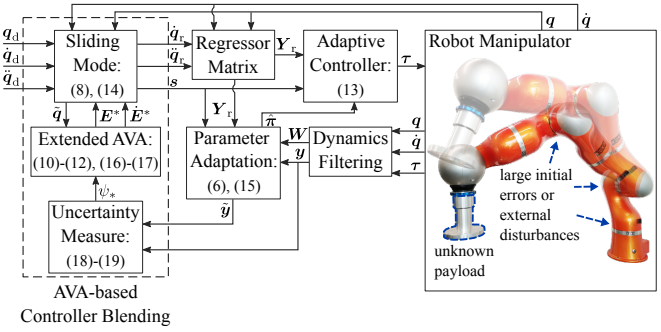

Fig. 1. Block diagram of the proposed adaptive control framework.

Learning-based [10]–[12] and model-free methods [13]–[15] have been developed to overcome the model discrepancy problem while achieving uncertainty-aware control action adjustment. In [10]–[12], Gaussian process regression (GPR) is applied to approximate the errors between the nominal and actual dynamics. The variance of the Gaussian processes (GPs) indicates the confidence of the predicted error model. It is thus utilized to directly modify the proportional-derivative (PD) gains [10], [11] or, together with the predicted mean of the GPs, to compute a robustness term [12]. The methods [13]–[15] completely cancel nonlinearities and unmodeled dynamics by using the time-delay estimation (TDE) technique. As the inertia-related gain matrix adapts, the effective PD gains are modified accordingly; however, the TDE error cannot influence the gain adaptation directly. Indeed, both aforementioned categories of methods are based on inverse dynamics, which may require excessive actuation to enforce the target linear dynamics of the closed loop [16].

On the other hand, to automatically achieve a trade-off between feasible control input and desired tracking performance, it is desirable that the feedback term of a controller can adapt depending on the error variables. This aspect has been addressed by self-tuning PD controllers based on fuzzy logic [17], [18], but they have the drawback of discontinuous gain switches. The adaptive variance algorithm (AVA) proposed in

Manuscript received: May 25, 2022; revised August 20, 2022; accepted September 19, 2022. This paper was recommended for publication by Editor Clement Gosselin upon evaluation of the Associate Editor and Reviewers' comments. This work was supported by ITECH R&D programs of MOTIE/KEIT under Grant 20014398. *(Corresponding author: Xuwei Wu.)*

X. Wu and A. Dietrich are with the Institute of Robotics and Mechatronics, German Aerospace Center (DLR), 82234 Wessling, Germany (e-mail: xuwei.wu@dlr.de).

A. Kirner and C. Ott are with the Automation and Control Institute, TU Wien, 1040 Vienna, Austria. C. Ott is also with the Institute of Robotics and Mechatronics, German Aerospace Center (DLR), 82234 Wessling, Germany.

G. Garofalo is with the ABB Corporate Research, 72178 Vasteras, Sweden.

P. Kotyczka is with the Chair of Automatic Control, Technical University of Munich (TUM), 85748 Garching, Germany.

Digital Object Identifier (DOI): see top of this page.

[19] achieves a smooth and state-dependent gain transition by using weighting functions. More specifically, the nominal feedback gain is multiplied by an unnormalized Gaussian function of the tracking error, which has an adaptive variance allowing the modified gain to eventually increase, thus ensuring the overall error convergence. In [20], AVA has been further extended for the application on robot manipulators. Moreover, rather than gain blending, this extension realizes a smooth controller blending between a global controller, which yields the desired compliant behavior when the system is far from the equilibrium point, and a local one, when the system is in a close neighborhood of the goal. Nevertheless, in both [19], [20] the precise knowledge of the system dynamics is assumed available, and AVA cannot modify its strategy accordingly in the presence of model uncertainties.

In this letter, we propose a novel passivity-based adaptive control framework, as shown in Fig. 1, to cope with dynamic parameter variations and to achieve an automatic feedback action transition depending on both error states and estimated model uncertainties. The framework uses the composite adaptive control scheme together with the natural adaptation law for parameter estimation. An uncertainty measure is computed via the prediction error of the composite adaptive controller and integrated into an extended AVA (eAVA), allowing an uncertainty-aware variance adaptation. As a result, the proposed control scheme can: 1) reduce the risk of actuator saturation under large tracking errors; 2) retain nominal feedback action to anticipate substantial modeling errors; 3) alleviate the parameter drift problem under external disturbances. The main contributions of this letter are:

- A new framework combining composite adaptive control and AVA with formally proved global convergence and boundedness properties.
- An extended AVA that automatically adjusts feedback action according to estimated model fidelity. A practical procedure for eAVA parameter tuning is also provided.
- Experimental validation and comparisons with the baseline schemes on a real robot under different types of modeling errors and external disturbances.

Notation: Throughout this letter, $|\cdot|$ denotes the absolute value of a real number and $\|\cdot\|$ the Euclidean norm of a vector. The notation $\mathcal{S}(p)$ stands for the space of real symmetric matrices $\boldsymbol{A} \in \mathbb{R}^{p\times p}$; $\mathcal{S}^+(p) \subset \mathcal{S}(p)$ additionally features positive definiteness. The operator $\mathrm{vech} : \mathcal{S}(p) \to \mathbb{R}^{p(p+1)/2}$ describes the vectorization of a symmetric matrix by using its distinctly different entries. For any $\boldsymbol{A} \in \mathcal{S}(p)$, its minimum and maximum eigenvalues are represented by $\lambda_{\mathrm{m}}(\boldsymbol{A}) \in \mathbb{R}$ and $\lambda_{\mathrm{M}}(\boldsymbol{A}) \in \mathbb{R}$, respectively. The identity matrix is denoted by $\boldsymbol{I}$ and the zero vector/matrix by $\boldsymbol{0}$; their dimensions can be retrieved from the context. A diagonal matrix with diagonal entries $\{A_1, \ldots, A_p\}$ is denoted by $\mathrm{diag}\{A_{1\ldots p}\} \in \mathbb{R}^{p\times p}$. A continuous function $\alpha : \mathbb{R}_{\geq 0} \to \mathbb{R}_{\geq 0}$ is of class $\mathcal{K}$, if it is strictly increasing and $\alpha(0) = 0$; $\alpha \in \mathcal{K}$ belongs to class $\mathcal{K}_\infty$, if it is also radially unbounded.

II. Fundamentals and Preliminaries

In this section we recall the basics of the natural adaptation law [4] for parameter estimation and AVA [20] for control action blending depending on tracking error.

A. Linear Parameterization of Robot Dynamics

The rigid-body dynamics of a fully-actuated robot with n degrees of freedom (DOF) can be written as

$$\boldsymbol{M}(\boldsymbol{q})\ddot{\boldsymbol{q}} + \boldsymbol{C}(\boldsymbol{q},\dot{\boldsymbol{q}})\dot{\boldsymbol{q}} + \boldsymbol{g}(\boldsymbol{q}) = \boldsymbol{\tau}\ , \tag{1}$$

where $\boldsymbol{q} \in \mathbb{R}^n$ denotes the joint positions; the inertia matrix $\boldsymbol{M}(\boldsymbol{q}) \in \mathcal{S}^+(n)$ and the Coriolis/centrifugal matrix $\boldsymbol{C}(\boldsymbol{q},\dot{\boldsymbol{q}}) \in \mathbb{R}^{n\times n}$ are assumed to satisfy the passivity property [21]; $\boldsymbol{g}(\boldsymbol{q}) \in \mathbb{R}^n$ is the generalized gravitational force, and $\boldsymbol{\tau} \in \mathbb{R}^n$ the motor input. In this work, we assume[1]:

Assumption 1: $\boldsymbol{M}(\boldsymbol{q})$ and $\boldsymbol{C}(\boldsymbol{q},\dot{\boldsymbol{q}})$ are uniformly bounded for all possible $\boldsymbol{q}$, and $\boldsymbol{C}(\boldsymbol{q},\dot{\boldsymbol{q}})$ is linear in $\dot{\boldsymbol{q}}$.

The dynamics (1) are known to be linearly parameterizable [21], i.e., $\boldsymbol{\tau} = \boldsymbol{Y}(\boldsymbol{q},\dot{\boldsymbol{q}},\ddot{\boldsymbol{q}})\boldsymbol{\pi}$, where $\boldsymbol{Y}(\boldsymbol{q},\dot{\boldsymbol{q}},\ddot{\boldsymbol{q}}) \in \mathbb{R}^{n\times 10n}$ is the regressor matrix, and $\boldsymbol{\pi} = [\boldsymbol{\pi}_1^T \ \ldots \ \boldsymbol{\pi}_n^T]^T \in \mathbb{R}^{10n}$ stacks the inertial parameter vectors of all links. Given the mass m_i, the center of mass $\boldsymbol{c}_i$, and the inertia tensor $\boldsymbol{\Theta}_i \in \mathcal{S}^+(3)$ of the i-th link, $\boldsymbol{\pi}_i \in \mathbb{R}^{10}$ is defined as

$$\boldsymbol{\pi}_i = \begin{bmatrix} m_i & m_i\boldsymbol{c}_i^T & \mathrm{vech}(\boldsymbol{\Theta}_i)^T \end{bmatrix}^T\ . \tag{2}$$

B. Natural Adaptation Law

The elements of $\boldsymbol{\pi}_i$ must satisfy a set of constraints such that the underlying mass distribution of the rigid link is physically realizable [5], [6], which is referred to as the physical-consistency condition. These constraints on $\boldsymbol{\pi}_i$ are equivalent to requiring the positive definiteness of the so-called pseudo-inertia matrix [24]

$$\boldsymbol{\Pi}_i = \varphi(\boldsymbol{\pi}_i) = \begin{bmatrix} m_i & m_i\boldsymbol{c}_i^T \\ m_i\boldsymbol{c}_i & \boldsymbol{\Sigma}_i \end{bmatrix} \in \mathcal{S}^+(4)\ , \tag{3}$$

where $\boldsymbol{\Sigma}_i = \frac{1}{2}\mathrm{tr}(\boldsymbol{\Theta}_i)\boldsymbol{I} - \boldsymbol{\Theta}_i \in \mathcal{S}(3)$. The inverse of the linear map $\varphi : \mathbb{R}^{10} \to \mathcal{S}(4)$ is given by

$$\varphi^{-1}(\boldsymbol{\Pi}_i) = \begin{bmatrix} m_i & m_i\boldsymbol{c}_i^T & \mathrm{vech}(\mathrm{tr}(\boldsymbol{\Sigma}_i)\boldsymbol{I} - \boldsymbol{\Sigma}_i)^T \end{bmatrix}^T\ . \tag{4}$$

The geometric structure of $\boldsymbol{\Pi}_i$ has been exploited in [4] to develop a pseudo-distance metric

$$D_{\mathcal{M}}(\boldsymbol{\pi}_{i,a},\boldsymbol{\pi}_{i,b}) = \log\left(\frac{\det(\boldsymbol{\Pi}_{i,b})}{\det(\boldsymbol{\Pi}_{i,a})}\right) + \mathrm{tr}(\boldsymbol{\Pi}_{i,b}^{-1}\boldsymbol{\Pi}_{i,a}) - 4 \tag{5}$$

on $\mathcal{M} \subset \mathbb{R}^{10}$, which represents the manifold of all possible physically consistent $\boldsymbol{\pi}_i$ for a single link. This new metric leads to the natural adaptation law given by [4]

$$\dot{\hat{\boldsymbol{\Pi}}}_i = -\gamma\hat{\boldsymbol{\Pi}}_i\boldsymbol{L}_i\hat{\boldsymbol{\Pi}}_i \tag{6}$$

for $i = 1, \ldots, n$, where $\hat{\boldsymbol{\Pi}}_i \in \mathcal{S}^+(4)$ is the current estimate of $\boldsymbol{\Pi}_i$; $\gamma > 0$ is the adaptation gain; $\boldsymbol{L}_i \in \mathcal{S}(4)$ is the unique solution of $\mathrm{tr}(\boldsymbol{\Pi}_i\boldsymbol{L}_i) = \boldsymbol{\pi}_i^T\boldsymbol{l}_i$ [7], [25]. The concrete expression of $\boldsymbol{l}_i \in \mathbb{R}^{10}$ will be shown for the proposed controller in Section III. As proved in [4], starting with a valid initial estimate $\hat{\boldsymbol{\Pi}}_i(t_0) \in \mathcal{S}^+(4)$, or equivalently, with $\hat{\boldsymbol{\pi}}_i(t_0) \in \mathcal{M}$, the

[1]This is satisfied, e.g., for all robots that feature only revolute or only prismatic joints [22], [23].

adaptation law (6) can ensure that $\hat{\boldsymbol{\pi}}_i(t) = \varphi^{-1}(\hat{\boldsymbol{\Pi}}_i(t)) \in \mathcal{M}$ for all time $t > t_0$. Compared to conventional adaptation laws [21] based on a quadratic error term, (6) requires only a scalar gain instead of a gain matrix, without suffering from possible scaling problems. Moreover, as shown in [4], it can largely improve the transient performance and provide better generalizability to varied reference trajectories.

C. Adaptive Variance Algorithm

When the precise knowledge of (1) is available, AVA can be integrated into the passivity-based controller [1] at position level, leading to [20]

$$\boldsymbol{\tau} = \boldsymbol{M}(\boldsymbol{q})\ddot{\boldsymbol{q}}_\mathrm{r} + \boldsymbol{C}(\boldsymbol{q},\dot{\boldsymbol{q}})\dot{\boldsymbol{q}}_\mathrm{r} + \boldsymbol{g}(\boldsymbol{q}) - \boldsymbol{H}\boldsymbol{s} \ , \tag{7}$$

in which $\boldsymbol{s} = \dot{\boldsymbol{q}} - \dot{\boldsymbol{q}}_r$ is the sliding variable, and

$$\dot{\boldsymbol{q}}_\mathrm{r} = \dot{\boldsymbol{q}}_\mathrm{d}(t) - \boldsymbol{E}\boldsymbol{K}\tilde{\boldsymbol{q}} + (\boldsymbol{I} - \boldsymbol{E})\boldsymbol{v}_\mathrm{g}(\tilde{\boldsymbol{q}}) \tag{8}$$

is the modified reference velocity. The vector $\tilde{\boldsymbol{q}} = \boldsymbol{q} - \boldsymbol{q}_\mathrm{d}(t)$ contains the joint position errors, and the desired trajectory $\boldsymbol{q}_\mathrm{d}(t)$ has continuous and bounded time derivatives $\dot{\boldsymbol{q}}_\mathrm{d}(t), \ddot{\boldsymbol{q}}_\mathrm{d}(t)$. The gain matrices $\boldsymbol{H} \in \mathbb{R}^{n\times n}$ and $\boldsymbol{K} = \mathrm{diag}\{K_{1\dots n}\}$ are positive definite. The so-called global controller $\boldsymbol{v}_\mathrm{g}(\tilde{\boldsymbol{q}}) \in \mathbb{R}^n$ is written as [20]

$$\boldsymbol{v}_\mathrm{g}(\tilde{\boldsymbol{q}}) = \begin{bmatrix} v_{\mathrm{g},1}(\tilde{q}_1) & \dots & v_{\mathrm{g},n}(\tilde{q}_n) \end{bmatrix}^T \ , \tag{9}$$

and it satisfies $\tilde{q}_i v_{\mathrm{g},i}(\tilde{q}_i) \le 0$, $\forall i = 1,\dots,n$. This global controller, in comparison with the local one $-\boldsymbol{K}\tilde{\boldsymbol{q}}$, aims at avoiding unfeasible control action for large tracking errors. The blending of the local and global controllers is realized in (8) through the weighting matrix

$$\boldsymbol{E} = \mathrm{diag}\{E_{1\dots n}\} \ ; \ E_i = \exp(-U_i) \ , \tag{10}$$

where the scalar function $U_i : \mathbb{R}\times\mathbb{R} \to \mathbb{R}_{\ge 0}$ is given by

$$U_i(\tilde{q}_i, \sigma_i) = \frac{\tilde{q}_i^2}{2(\bar{\sigma}_i^2 + \sigma_i^2)} \tag{11}$$

with $\bar{\sigma}_i > 0$ being a constant parameter. In view of (11), each E_i represents an unnormalized, unimodal Gaussian function with zero mean. When q_i largely deviates from its desired trajectory, i.e., $\tilde{q}_i^2 \gg \bar{\sigma}_i^2 + \sigma_i^2$, the function E_i will decrease, leading to the dominance of $v_{\mathrm{g},i}(\tilde{q}_i)$ in (8). Moreover, the variance of E_i can be adjusted by the internal state σ_i. The dynamic equations of $\boldsymbol{\sigma} = [\sigma_1 \ \dots \ \sigma_n]^T \in \mathbb{R}^n$ are defined as

$$\dot{\boldsymbol{\sigma}} = (\boldsymbol{K}_\sigma^\mathrm{l} - \boldsymbol{E}\boldsymbol{K}_\sigma^\mathrm{h})\boldsymbol{\sigma} \ , \tag{12}$$

where $\boldsymbol{K}_\sigma^\mathrm{l} = \mathrm{diag}\{K_{\sigma,1\dots n}^\mathrm{l}\}, \boldsymbol{K}_\sigma^\mathrm{h} = \mathrm{diag}\{K_{\sigma,1\dots n}^\mathrm{h}\}$ are positive definite, and $K_{\sigma,i}^\mathrm{l} < K_{\sigma,i}^\mathrm{h}$, $\forall i = 1,\dots,n$. If $\tilde{q}_i$ remains large, σ_i will increase exponentially due to $K_{\sigma,i}^\mathrm{l} > E_i K_{\sigma,i}^\mathrm{h}$. Consequently, the variance of E_i expands, thereby triggering a control action transition towards $-K_i\tilde{q}_i$. Otherwise, when $\tilde{q}_i \approx 0$, the variance converges exponentially to $\bar{\sigma}_i^2$.

III. Control Design

In this section, we present a novel adaptive control framework combining the composite adaptive controller, the natural parameter adaptation, and the AVA-based feedback action blending. Furthermore, we propose an extended AVA that allows an variance adaptation according to estimated model uncertainties.

A. Combining Composite Adaptive Controller with AVA

The control design starts with replacing the ideal dynamic matrices in (7) by the respective estimates, denoted by $\hat{(\cdot)}$, leading to the control law

$$\begin{aligned}\boldsymbol{\tau} &= \hat{\boldsymbol{M}}(\boldsymbol{q})\ddot{\boldsymbol{q}}_\mathrm{r} + \hat{\boldsymbol{C}}(\boldsymbol{q},\dot{\boldsymbol{q}})\dot{\boldsymbol{q}}_\mathrm{r} + \hat{\boldsymbol{g}}(\boldsymbol{q}) - \boldsymbol{H}\boldsymbol{s} \\ &= \boldsymbol{Y}_\mathrm{r}\hat{\boldsymbol{\pi}} - \boldsymbol{H}\boldsymbol{s} \ ,\end{aligned} \tag{13}$$

where $\boldsymbol{Y}_\mathrm{r} = \boldsymbol{Y}(\boldsymbol{q},\dot{\boldsymbol{q}},\dot{\boldsymbol{q}}_\mathrm{r},\ddot{\boldsymbol{q}}_\mathrm{r})$, and $\ddot{\boldsymbol{q}}_\mathrm{r}$ is obtained by differentiating (8) with respect to time:

$$\ddot{\boldsymbol{q}}_\mathrm{r} = \ddot{\boldsymbol{q}}_\mathrm{d}(t) - \dot{\boldsymbol{E}}(\boldsymbol{K}\tilde{\boldsymbol{q}} + \boldsymbol{v}_\mathrm{g}(\tilde{\boldsymbol{q}})) - \boldsymbol{E}\boldsymbol{K}\dot{\tilde{\boldsymbol{q}}} + (\boldsymbol{I} - \boldsymbol{E})\dot{\boldsymbol{v}}_\mathrm{g} \ . \tag{14}$$

In (13), $\boldsymbol{H}$ is required to be uniformly continuous if it is time-varying [21]. Moreover, an additional assumption about $\boldsymbol{v}_\mathrm{g}(\tilde{\boldsymbol{q}})$, compared to [20], is made as follows[2]:

Assumption 2: For $i = 1,\dots,n$, $\partial v_{\mathrm{g},i}(\tilde{q}_i)/\partial\tilde{q}_i$ is uniformly bounded; $\partial v_{\mathrm{g},i}(\tilde{q}_i)/\partial\tilde{q}_i \le -\bar{K}_{\mathrm{g},i}$ holds with some $\bar{K}_{\mathrm{g},i} > 0$.

Here, the former condition implies that $v_{\mathrm{g},i}(\tilde{q}_i)$ is locally Lipschitz continuous, and the latter ensures that when linearized, $v_{\mathrm{g},i}(\tilde{q}_i)$ has a negative gradient everywhere on $\mathbb{R}$.

For the parameter adaptation, we adopt the composite adaptive controller [3] instead of the direct scheme [1] for two main reasons: 1) as shown in [21], smoother and faster parameter convergence can be achieved through the use of both the prediction and the tracking error in adaptation laws; 2) the prediction error is needed to compute an uncertainty measure, which is integrated in our proposed eAVA, as will be shown in Section III-B. Let $\boldsymbol{W}(\boldsymbol{q},\dot{\boldsymbol{q}})$ and $\boldsymbol{y}$ be the first-order low-pass filtered version of $\boldsymbol{Y}(\boldsymbol{q},\dot{\boldsymbol{q}},\ddot{\boldsymbol{q}})$ and $\boldsymbol{\tau}$, respectively. The prediction error is defined as $\tilde{\boldsymbol{y}} = \boldsymbol{W}\hat{\boldsymbol{\pi}} - \boldsymbol{y} = \boldsymbol{W}\tilde{\boldsymbol{\pi}}$ with $\tilde{\boldsymbol{\pi}} = \hat{\boldsymbol{\pi}} - \boldsymbol{\pi}$. The matrix $\boldsymbol{L}_i$ in (6) is then determined by solving [7]

$$\sum_{i=1}^{n} \mathrm{tr}(\boldsymbol{\Pi}_i\boldsymbol{L}_i) = \boldsymbol{\pi}^T(\boldsymbol{Y}_\mathrm{r}^T\boldsymbol{s} + \kappa\boldsymbol{W}^T\tilde{\boldsymbol{y}}) \ , \tag{15}$$

where the gain parameter $\kappa > 0$ weights the contributions of the prediction errors to the adaptation law.

B. Extending AVA with Uncertainty Measure

The original variance adaptation of [19], [20], as explained in Section II-C, is governed by the internal states $\boldsymbol{\sigma}$, whose dynamics (12) depend implicitly on the tracking errors via the Gaussian functions. Nevertheless, this strategy does not consider the critical influence of the modeling errors on tracking performance. Indeed, the feedforward-like compensation $\boldsymbol{Y}_\mathrm{r}\hat{\boldsymbol{\pi}}$ in (13) relies on an accurate estimation of $\boldsymbol{\pi}$. If the parameter estimation errors are considerably large, e.g., when the parameter adaptation just begins, the tracking performance may be severely degraded. Moreover, the low-gain nature of AVA under large control errors can further worsen the performance, at least temporarily. Although the global-to-local feedback action transition, triggered by an expanded variance, can eventually improve the performance, this transition only

[2]For example, a simple proportional controller $v_{\mathrm{g},i}(\tilde{q}_i) = -\bar{K}_{\mathrm{g},i}\tilde{q}_i$ or a modified sigmoid function $v_{\mathrm{g},i}(\tilde{q}_i) = -\bar{\tau}_i\tanh(\bar{K}_{\mathrm{g},i}\tilde{q}_i/\bar{\tau}_i) - \bar{K}_{\mathrm{g},i}\tilde{q}_i$ with $\bar{\tau}_i, \bar{K}_{\mathrm{g},i} > 0$ and $\bar{K}_{\mathrm{g},i} \ll \bar{K}_{\mathrm{g},i} \ll K_i$, $\forall i = 1,\dots,n$, satisfies Assumption 2.

happens *after* large tracking errors have already arisen. To overcome the above problem, we propose to integrate an uncertainty measure in the variance adaptation of AVA. The resulted eAVA allows the Gaussian functions to automatically expand in order to counteract substantial modeling errors *before* the occurrence of large tracking errors. The extension of (10)–(11) is defined as

$$\boldsymbol{E}^* = \mathrm{diag}\{E_{1\dots n}^*\} \ ; \ E_i^* = \exp(-U_i^*) \ , \tag{16}$$

$$U_i^*(\tilde{q}_i, \sigma_i, \psi_*) = \frac{\tilde{q}_i^2}{2(\bar{\sigma}_i^2 + \sigma_i^2 + a_i\psi_*)} \ , \tag{17}$$

where $a_i > 0$ is a design parameter, and $\psi_* \in \mathbb{R}$ is the uncertainty measure computed by

$$\dot{\psi}_* = -\frac{1}{T}(\psi_* - \psi(t, \tilde{\boldsymbol{y}}, \boldsymbol{y})) \ ; \ \psi_*(t_0) = 0 \ . \tag{18}$$

In other words, $\psi(t, \tilde{\boldsymbol{y}}, \boldsymbol{y})$ is low-pass filtered with the time constant $T > 0$ to obtain ψ_*. The function $\psi(t, \tilde{\boldsymbol{y}}, \boldsymbol{y})$ is introduced as

$$\psi(t, \tilde{\boldsymbol{y}}, \boldsymbol{y}) = \frac{\tilde{\boldsymbol{y}}^T \boldsymbol{Q} \tilde{\boldsymbol{y}}}{\boldsymbol{y}^T \boldsymbol{Q} \boldsymbol{y} + \bar{y}} \ , \tag{19}$$

where $\bar{y} > 0$ prevents the division by zero; $\boldsymbol{Q} \in \mathbb{R}^{n \times n}$ is (uniformly) positive semi-definite. Recall that $\tilde{\boldsymbol{y}}$ describes the low-pass filtered residual difference between the predicted output and the measured input of the dynamics (1). Hence, (19) provides a reasonably normalized measure indicating the relative impact of the modeling errors on the total system input. Moreover, the matrix $\boldsymbol{Q}$ can be freely chosen to allow further modifications, e.g., to only consider the prediction errors of specific links. Note that $\psi(t, \tilde{\boldsymbol{y}}, \boldsymbol{y})$ is uniformly bounded in $\tilde{\boldsymbol{y}}$ by definition, and the first-order filter (18) is exponentially stable and strictly proper. Thus, ψ_* and $\dot{\psi}_*$ are ensured to be bounded if $\tilde{\boldsymbol{y}}$ is bounded [21]. Furthermore, since $\psi(t, \tilde{\boldsymbol{y}}, \boldsymbol{y})$ is positive semi-definite in $\tilde{\boldsymbol{y}}$, if $\tilde{\boldsymbol{y}} \to \boldsymbol{0}$ then $\psi_* \to 0$, and consequently, (17) simplifies to (11) of the original AVA. Fig. 2 illustrates the behaviors of E_i and E_i^*.

C. Tuning eAVA Parameters

The variance adaptation mechanism in (10)–(12) and (16)–(17) involves the design parameters $\bar{\sigma}_i, K_{\sigma,i}^{\mathrm{l}}, K_{\sigma,i}^{\mathrm{h}}, a_i$ for each joint. A direct tuning of these parameters is usually not intuitive and can be challenging for multi-DOF systems. Therefore, a practical procedure for the eAVA parameter tuning is introduced here. First, let $\nu_i \in (0, 1)$ denote the ratio $K_{\sigma,i}^{\mathrm{l}}/K_{\sigma,i}^{\mathrm{h}}$. In view of (12), σ_i will increase when $E_i < \nu_i$. The boundary value of $|\tilde{q}_i|$ when $E_i = \nu_i$ and $\sigma_i = 0$, is given by $\breve{q}_i = \bar{\sigma}_i\sqrt{2|\ln(\nu_i)|}$. This positive constant represents a user-defined threshold: if $|\tilde{q}_i|$ stays below $\breve{q}_i$ throughout the trajectory tracking, the internal state σ_i can never increase to expand the variance of both Gaussian functions E_i and E_i^*. Meanwhile, the weighting coefficient of the nominal feedback action is ensured to be at a minimum of ν_i. Upon selection of ν_i and $\breve{q}_i$, one obtains

$$\bar{\sigma}_i = \frac{\breve{q}_i}{\sqrt{2|\ln(\nu_i)|}} \ . \tag{20}$$

Second, recall that ψ_* in (17) aims at retaining a certain amount of nominal feedback action, independently from σ_i, in order to counteract considerable model discrepancies. Hence, one can select a desired weighting coefficient $E_i^* = \nu_i^* \geq \nu_i$ of the nominal feedback action, when $|\tilde{q}_i| = \breve{q}_i$, $\sigma_i = 0$, and $\psi_* = \bar{\psi}_*$. The new parameter $\bar{\psi}_*$ describes another user-defined threshold: once ψ_* exceeds $\bar{\psi}_*$, a weighting coefficient no less than ν_i^* will be restored even when $|\tilde{q}_i| \leq \breve{q}_i$. Note that when $|\tilde{q}_i| \leq \breve{q}_i$, the global-to-local control action transition cannot be started by the internal state. With ν_i^* and $\bar{\psi}_*$ determined, a_i is given by

$$a_i = \frac{\breve{q}_i^2 - 2\bar{\sigma}_i^2|\ln(\nu_i^*)|}{2\bar{\psi}_*|\ln(\nu_i^*)|} = \frac{\breve{q}_i^2(1 - \frac{|\ln(\nu_i^*)|}{|\ln(\nu_i)|})}{2\bar{\psi}_*|\ln(\nu_i^*)|} \ . \tag{21}$$

Note that the auxiliary parameters ν_i, $\breve{q}_i$, $\bar{\psi}_*$, and ν_i^*, are merely introduced for tuning eAVA, and they do not affect any conclusions of the following stability analysis.

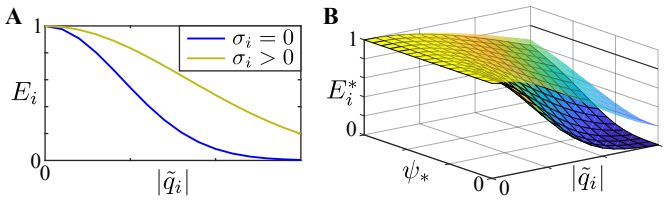

Fig. 2. Illustration of the Gaussian functions with fixed σ_i. **A**: E_i of the original AVA used in [19], [20]. **B**: E_i^* of the proposed eAVA with the uncertainty measure ψ_*; the semi-transparent surface represents the case $\sigma_i > 0$.

D. Stability Analysis

The closed-loop system can be obtained as

$$\boldsymbol{M}\dot{\boldsymbol{s}} + (\boldsymbol{C} + \boldsymbol{H})\boldsymbol{s} = \boldsymbol{Y}_{\mathrm{r}}\tilde{\boldsymbol{\pi}} \ , \tag{22a}$$

$$\dot{\hat{\boldsymbol{\Pi}}}_i = -\gamma\hat{\boldsymbol{\Pi}}_i\boldsymbol{L}_i\hat{\boldsymbol{\Pi}}_i \ , \tag{22b}$$

$$\dot{\tilde{\boldsymbol{q}}} = -\boldsymbol{E}^*\boldsymbol{K}\tilde{\boldsymbol{q}} + (\boldsymbol{I} - \boldsymbol{E}^*)\boldsymbol{v}_{\mathrm{g}}(\tilde{\boldsymbol{q}}) + \boldsymbol{s} \ , \tag{22c}$$

$$\dot{\boldsymbol{\sigma}} = (\boldsymbol{K}_\sigma^{\mathrm{l}} - \boldsymbol{E}\boldsymbol{K}_\sigma^{\mathrm{h}})\boldsymbol{\sigma} \ , \tag{22d}$$

$$\dot{\psi}_* = -\frac{1}{T}(\psi_* - \psi(t, \tilde{\boldsymbol{y}}, \boldsymbol{y})) \ , \tag{22e}$$

by applying (13) to (1) and by modifying (8) through (16)–(17) together with (18)–(19). Note that (22d) is not influenced by the uncertainty measure, because $\boldsymbol{\sigma}$ and ψ_* are considered as independent driving forces for the variance adaptation. The main results of the stability analysis are summarized in the following proposition.

Proposition 1: Consider the closed-loop system (22) *under Assumptions 1 and 2. Suppose that the real inertial parameters* $\boldsymbol{\pi}$ *remain constant during trajectory tracking. Then, the terms* $\boldsymbol{s}, \tilde{\boldsymbol{q}}, \dot{\tilde{\boldsymbol{q}}}, \tilde{\boldsymbol{y}}, \boldsymbol{\sigma}, \dot{\boldsymbol{\sigma}}$ *converge to zero;* $\tilde{\boldsymbol{\pi}}$ *is uniformly globally bounded on*[3] $\mathcal{M}^{(n)}$.

Proof: The proof consists of four major steps, in which the subsequent conclusions will be established:

① Boundedness of $\boldsymbol{s}, \tilde{\boldsymbol{\pi}}$;
② Boundedness of $\tilde{\boldsymbol{q}}, \dot{\tilde{\boldsymbol{q}}}, \boldsymbol{\sigma}, \dot{\boldsymbol{\sigma}}$;
③ Boundedness of $\dot{\boldsymbol{q}}_{\mathrm{r}}, \ddot{\boldsymbol{q}}_{\mathrm{r}}, \tilde{\boldsymbol{y}}, \dot{\tilde{\boldsymbol{y}}}, \psi_*, \dot{\psi}_*, \dot{\boldsymbol{s}}$;
④ Convergence of $\boldsymbol{s}, \tilde{\boldsymbol{q}}, \dot{\tilde{\boldsymbol{q}}}, \tilde{\boldsymbol{y}}, \boldsymbol{\sigma}, \dot{\boldsymbol{\sigma}} \to \boldsymbol{0}$.

[3]For a multi-DOF system with n rigid links, the space of all physically consistent $\boldsymbol{\pi}$ is denoted by $\mathcal{M}^{(n)}$.

Step ①: As in [4], a continuously differentiable function $V : \mathbb{R}_{\geq t_0} \times \mathbb{R}^n \times \mathcal{M}^{(n)} \to \mathbb{R}_{\geq 0}$ can be defined as

$$V(t, \boldsymbol{s}, \tilde{\boldsymbol{\pi}}) = \frac{1}{2}\boldsymbol{s}^T\boldsymbol{M}\boldsymbol{s} + \frac{1}{\gamma}\sum_{i=1}^{n} D_{\mathcal{M}}(\boldsymbol{\pi}_i, \overbrace{\tilde{\boldsymbol{\pi}}_i + \hat{\boldsymbol{\pi}}_i}^{\hat{\boldsymbol{\pi}}_i}) \ , \quad (23)$$

where the latter term, denoted by $V_{\mathrm{p}}(\tilde{\boldsymbol{\pi}})$, is based on the pseudo-distance metric (5) on $\mathcal{M}$, and it is positive definite in $\tilde{\boldsymbol{\pi}}$. Moreover, due to Assumption 1, $V(t, \boldsymbol{s}, \tilde{\boldsymbol{\pi}})$ satisfies

$$\frac{1}{2}\lambda_{\mathrm{m}}(\boldsymbol{M})\boldsymbol{s}^T\boldsymbol{s} + V_p \leq V \leq \frac{1}{2}\lambda_{\mathrm{M}}(\boldsymbol{M})\boldsymbol{s}^T\boldsymbol{s} + V_p \ . \quad (24)$$

Furthermore, one can obtain the time derivative of V as

$$\begin{aligned}\dot{V} &= \boldsymbol{s}^T(\boldsymbol{Y}_r\tilde{\boldsymbol{\pi}} - \boldsymbol{H}\boldsymbol{s}) + \frac{1}{\gamma}\sum_{i=1}^{n}\mathrm{tr}(\hat{\boldsymbol{\Pi}}_i^{-1}\dot{\hat{\boldsymbol{\Pi}}}_i\hat{\boldsymbol{\Pi}}_i^{-1}\tilde{\boldsymbol{\Pi}}_i) \\ &= -\boldsymbol{s}^T\boldsymbol{H}\boldsymbol{s} - \kappa\tilde{\boldsymbol{y}}^T\tilde{\boldsymbol{y}} \leq 0 \ , \end{aligned} \quad (25)$$

by using the skew-symmetry of $\dot{\boldsymbol{M}} - 2\boldsymbol{C}$ and applying (15) together with the symmetry of $\tilde{\boldsymbol{\Pi}}_i\boldsymbol{L}_i$. From (23)–(25), one can infer the uniform global boundedness of $\boldsymbol{s}$ and $\tilde{\boldsymbol{\pi}}$ [26, Theorem 1]; the uniformity holds because V_p, $\lambda_{\mathrm{m}}(\boldsymbol{M})$, and $\lambda_{\mathrm{M}}(\boldsymbol{M})$ in (24) are all independent of time.

Step ②: The main results reported in [27], see Theorem 1 in Appendix, will be used to conclude the input-to-state stability (ISS) of the subsystem (22c)–(22d) with respect to the state $[\tilde{\boldsymbol{q}}^T, \boldsymbol{\sigma}^T]^T$ and the input[4] $\boldsymbol{s}$. Due to the diagonal structure of this subsystem, each DOF of (22c)–(22d) is an interconnection (33a)–(33b) with $\boldsymbol{x}_1 = \tilde{q}_i$, $\boldsymbol{x}_2 = \sigma_i$, $\boldsymbol{u}_1 = s_i$, and $\boldsymbol{u}_2 = 0$. Note that the local Lipschitz condition is fulfilled due to Assumption 2. For the i-th subsystem of (22c), consider the ISS Lyapunov function candidate $V_1(\tilde{q}_i) = \tilde{q}_i^2/2$. Differentiating V_1 with respect to time yields

$$\begin{aligned}\dot{V}_1 &= -E_i^*K_i\tilde{q}_i^2 + (1 - E_i^*)\tilde{q}_i v_{\mathrm{g},i}(\tilde{q}_i) + \tilde{q}_i s_i \\ &\leq \tilde{q}_i v_{\mathrm{g},i}(\tilde{q}_i) + \tilde{q}_i s_i \ , \end{aligned} \quad (26)$$

since $\tilde{q}_i v_{\mathrm{g},i}(\tilde{q}_i) \leq 0$ and $E_i^* \in (0, 1]$ hold. In view of Assumption 2, it can be shown that $\tilde{q}_i v_{\mathrm{g},i}(\tilde{q}_i) \leq -\bar{K}_{\mathrm{g},i}\tilde{q}_i^2$. Then, using Young's inequality, one obtains

$$\dot{V}_1 \leq -\bar{K}_{\mathrm{g},i}\tilde{q}_i^2 + \frac{c_1\tilde{q}_i^2}{2} + \frac{s_i^2}{2c_1} \ , \quad \forall c_1 > 0 \ . \quad (27)$$

Let $c_1 \in (0, 2\bar{K}_{\mathrm{g},i})$, it follows that with $\theta \in (0, \bar{K}_{\mathrm{g},i} - c_1/2)$,

$$\forall \tilde{q}_i^2 \geq \frac{s_i^2}{2c_1\theta} \ , \quad \dot{V}_1 \leq -(\bar{K}_{\mathrm{g},i} - \frac{c_1}{2} - \theta)\tilde{q}_i^2 \ . \quad (28)$$

Let $\alpha_1 \in \mathcal{K}_\infty$ and $\rho_1 \in \mathcal{K}$ be defined as

$$\alpha_1(r) = 2(\bar{K}_{\mathrm{g},i} - \frac{c_1}{2} - \theta)r \ , \quad \rho_1(r) = \frac{r^2}{4c_1\theta} \ . \quad (29)$$

In view of (28), one can show that $V_1(\tilde{q}_i) \geq \rho_1(|s_i|)$ implies $\dot{V}_1 \leq -\alpha_1(V_1)$, which holds for all possible $\chi_1 \in \mathcal{K}$, see condition 2) in Theorem 1. Next, for the i-th subsystem of (22d), an ISS Lyapunov function candidate can be chosen as $V_2(\sigma_i) = \sigma_i^2/2$ [19]. If α_2 and χ_2 are selected as

$$\alpha_2(r) = c_2 r \ , \quad \chi_2(r) = \frac{r}{2\left|\ln(\frac{2K_{\sigma,i}^{\mathrm{l}} + c_2}{2K_{\sigma,i}^{\mathrm{h}}})\right|} \quad (30)$$

with $0 < c_2 < 2(K_{\sigma,i}^{\mathrm{h}} - K_{\sigma,i}^{\mathrm{l}})$, then $V_2(\sigma_i) \geq \chi_2(V_1)$ implies $\dot{V}_2 \leq -\alpha_2(V_2)$, see [19, Proof of Theorem 1]. Since χ_1 can be chosen arbitrarily, it is always possible to find a value that fulfills $\chi_1 \circ \chi_2(r) < r$, $\forall r > 0$. Therefore, based on Theorem 1, the subsystem (22c)–(22d) is input-to-state-stable with respect to the input $\boldsymbol{s}$. This leads to the uniform global boundedness of $\tilde{\boldsymbol{q}}, \dot{\tilde{\boldsymbol{q}}}, \boldsymbol{\sigma}, \dot{\boldsymbol{\sigma}}$ upon that of $\boldsymbol{s}$, which has already been shown in step ①.

Step ③: From the results of steps ①–②, it is clear that $\dot{\boldsymbol{q}}_{\mathrm{r}} = \dot{\boldsymbol{q}} - \boldsymbol{s}$ and $\tilde{\boldsymbol{y}} = \boldsymbol{W}\tilde{\boldsymbol{\pi}}$ are bounded; consequently, ψ_* and $\dot{\psi}_*$ are bounded according to (22e). Replacing $\boldsymbol{E}, \dot{\boldsymbol{E}}$ with $\boldsymbol{E}^*, \dot{\boldsymbol{E}}^*$ in (14), respectively, it remains to show that all $\dot{v}_{\mathrm{g},i}$ and $\dot{U}_i^*$ for $i = 1, \ldots, n$ are bounded in order to conclude the boundedness of $\ddot{\boldsymbol{q}}_{\mathrm{r}}$. Based on Assumption 2 and the boundedness of $\tilde{\boldsymbol{q}}$ and $\dot{\tilde{\boldsymbol{q}}}$, $\dot{v}_{\mathrm{g},i} = \frac{\partial v_{\mathrm{g},i}(\tilde{q}_i)}{\partial \tilde{q}_i}\dot{\tilde{q}}_i$ is bounded. Moreover, $\dot{U}_i^*$ can be written as

$$\dot{U}_i^* = \frac{\tilde{q}_i\dot{\tilde{q}}_i}{\bar{\sigma}_i^2 + \sigma_i^2 + a_i\psi_*} - \frac{\tilde{q}_i^2(2\sigma_i\dot{\sigma}_i + a_i\dot{\psi}_*)}{2(\bar{\sigma}_i^2 + \sigma_i^2 + a_i\psi_*)^2} \ , \quad (31)$$

whose boundedness can be easily shown. Thus, $\ddot{\boldsymbol{q}}_{\mathrm{r}}$ is bounded; in turn, $\boldsymbol{Y}_{\mathrm{r}}$ is bounded. Based on (22a), $\dot{\boldsymbol{s}}$ is bounded under Assumption 1 and the established boundedness conditions. Furthermore, differentiating $\tilde{\boldsymbol{y}}$ with respect to time yields $\dot{\tilde{\boldsymbol{y}}} = \boldsymbol{W}\dot{\tilde{\boldsymbol{\pi}}} + \dot{\boldsymbol{W}}\tilde{\boldsymbol{\pi}}$. Note that $\boldsymbol{L}_i$ is bounded since the right-hand side of (15) is bounded. Hence, $\dot{\hat{\boldsymbol{\pi}}}_i = \varphi^{-1}(-\gamma\hat{\boldsymbol{\Pi}}_i\boldsymbol{L}_i\hat{\boldsymbol{\Pi}}_i)$ is guaranteed to be bounded. Finally, the boundedness of $\dot{\boldsymbol{W}}$ is obvious due to its stable first-order differential equation [3] with $\boldsymbol{Y}(\boldsymbol{q}, \dot{\boldsymbol{q}}, \ddot{\boldsymbol{q}})$ as input, which is itself bounded[5]. Hence, $\dot{\tilde{\boldsymbol{y}}}$ is bounded.

Step ④: The time derivative of $\dot{V}$ can be expressed as

$$\ddot{V} = -\boldsymbol{s}^T\boldsymbol{H}\dot{\boldsymbol{s}} - \dot{\boldsymbol{s}}^T\boldsymbol{H}\boldsymbol{s} - \boldsymbol{s}^T\dot{\boldsymbol{H}}\boldsymbol{s} - 2\kappa\tilde{\boldsymbol{y}}^T\dot{\tilde{\boldsymbol{y}}} \ . \quad (32)$$

As all terms on the right-hand side of (32) remain bounded, $\ddot{V}$ is bounded, which assures the uniform continuity of $\dot{V}$. According to Barbalat's lemma [21], this implies that $\dot{V} \to 0$ as $t \to \infty$; consequently, $\boldsymbol{s}, \tilde{\boldsymbol{y}} \to \boldsymbol{0}$ as $t \to \infty$, as seen from (25). Due to the ISS of (22c)–(22d) with respect to $\boldsymbol{s}$, one can further conclude that $\tilde{\boldsymbol{q}}, \boldsymbol{\sigma} \to \boldsymbol{0}$ as $t \to \infty$. The convergence of $\dot{\tilde{\boldsymbol{q}}} = \dot{\boldsymbol{\sigma}} = \boldsymbol{0}$ can be established in view of (22c)–(22d). ■

Remark 1: The above proof can be straightforwardly extended for two cases: 1)[6] when eAVA also modifies the control action corresponding to $\boldsymbol{s}$, similarly to [20]; 2) when the original AVA is combined with a direct [1] or composite adaptive controller [3].

IV. Experimental Validation

The proposed framework is validated through three experiments on a KUKA LWR IV+ with seven torque-controlled

[4]Note that all subsequent statements in step ② are valid regardless of the input ψ_* (via $\boldsymbol{E}^*$) to the subsystem (22c); thus, this input is not considered in the analysis of step ② to simplify the proof without loss of generality.

[5]Note that all $\boldsymbol{q} = \tilde{\boldsymbol{q}} + \boldsymbol{q}_{\mathrm{d}}(t)$, $\dot{\boldsymbol{q}} = \boldsymbol{s} + \dot{\boldsymbol{q}}_{\mathrm{r}}$, $\ddot{\boldsymbol{q}} = \dot{\boldsymbol{s}} + \ddot{\boldsymbol{q}}_{\mathrm{r}}$ are bounded.

[6]Provided that a diagonal $\boldsymbol{H}$ is assigned, and the global controller of $\boldsymbol{s}$ satisfies Assumption 2.

TABLE I
CONSTANT CONTROL PARAMETERS

Experiments	K_i	$K_{\mathrm{g},i}$	$K^{\mathrm{l}}_{\sigma,i}$	γ	κ
#1 Regulation	10	1	5	0.3	0.05
#2 Tracking	20	2	10	0.3* / 0.05†	0.05* / 0.02†
#3 Ext. Disturb.	10	0.5	5	1.4	0.02

* With an unknown payload at the end-effector
† Under mass parameter variations of all links

DOF ($n = 7$), as shown in Fig. 1. The same nominal proportional gain K_i is chosen for all joints, and $\boldsymbol{H} = \boldsymbol{K}\hat{\boldsymbol{M}}$ is applied to assign higher gains to links with larger inertia, as recommended in [21]. Note that the positive definiteness of $\hat{\boldsymbol{M}}$ is guaranteed by the natural adaptation law. As the global controller, $v_{\mathrm{g},i}(\tilde{q}_i) = -K_{\mathrm{g},i}\tilde{q}_i$ is used for all joints. The control parameters are reported in Table I. For all experiments, the auxiliary parameters introduced in Section III-C are empirically chosen as $\breve{q}_i = 0.07$, $\nu_i = 0.3$, and $\nu_i^* = 0.7$ for $i = 1, \ldots, 7$, from which the AVA parameters $K^{\mathrm{h}}_{\sigma,i}$ and $\bar{\sigma}_i$ can be derived. Moreover, in order to evaluate the proposed eAVA, i.e., with (16)–(19), different values of a_i over $\{0.21, 0.12, 0.08, 0.04\}$ are tested by setting $\bar{\psi}_*^{1/2}$ to $\{0.15, 0.2, 0.25, 0.35\}$, respectively. The prediction error of each joint contributes equally to the uncertainty measure by selecting $\boldsymbol{Q} = \boldsymbol{I}$. The time constants of the low-pass filters that provide $\tilde{\boldsymbol{y}}$ and ψ_* are set to $1/6\,\mathrm{s}$ and $1/3.14\,\mathrm{s}$, respectively. The regressor matrices, i.e., $\boldsymbol{Y}_{\mathrm{r}}$ and $\boldsymbol{W}$, are computed using the recursive formulation in [28]. All components of the proposed framework run at the same sampling rate of $1\,\mathrm{kHz}$.

For comparison, three baseline approaches are considered: 1) the composite adaptive controller with constant gains (CA); 2) the original AVA [20]; 3) the direct combination of CA with AVA (CA+AVA). The proposed framework is denoted by CA+eAVA in the following. AVA and CA+AVA are tested using the same control and auxiliary parameters[7] as CA+eAVA. An accompanying video shows all experiments.

A. Experiment #1: Regulation with an Unknown Payload

The first experiment shows the capability of the proposed framework to perform a regulation task with an unknown payload at the end-effector (see Fig. 1) and large initial position errors. To this end, the joints 1, 2, and 4 have an absolute, initial deviation of $0.14\,\mathrm{rad}$ each with respect to their goal positions. The results are shown in Fig. 3. Without the feedback action blending of AVA, CA generates excessive control input (Fig. 3C); the maximum Euclidean norm of the commanded torques is $114\,\mathrm{Nm}$. In contrast, all approaches using AVA or eAVA successfully avoid high control input. The shaded rectangles in Fig. 3 highlight the time period when ψ_* increases from zero to its maximum during the transient (Fig. 3F). As expected, the proposed eAVA reacts directly to the substantial model uncertainties detected by ψ_* (Fig. 3B). Consequently, the proposed CA+eAVA can partially regain the nominal feedback action prior to the rise of σ_i (Fig. 3D) and achieves a better overall performance compared to CA+AVA

[7]Except for a_i, ν_i^*, and $\bar{\psi}_*$, which are only needed in eAVA.

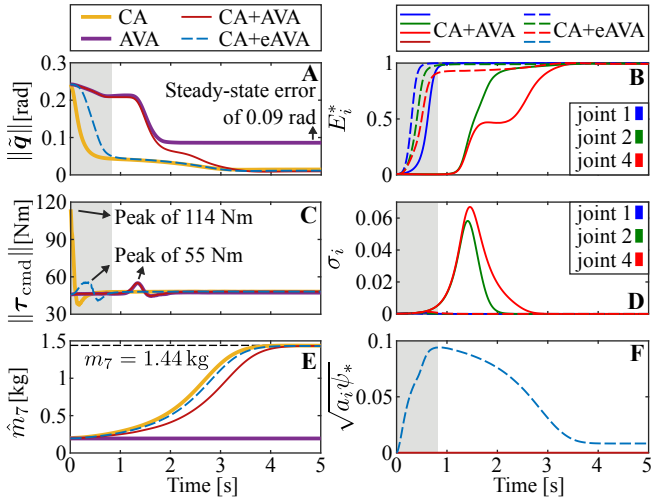

Fig. 3. Experiment #1: Regulation case with an unknown payload at the end-effector. Here, $\boldsymbol{\tau}_{\mathrm{cmd}}$ denotes the commanded torques, and $\hat{m}_7$ the estimated mass of the last link. The absolute initial position error on the joints 1, 2, and 4 is $0.14\,\mathrm{rad}$ each. The total mass of the last link including the payload is approximated as $m_7 = 1.44\,\mathrm{kg}$ through available CAD data. For CA+eAVA, $a_i = 0.21$ is selected, and the shaded rectangles highlight the time interval when ψ_* increases from zero to its maximum value.

(Fig. 3A). On the other hand, the parameter adaptation of all approaches using CA achieves a good and comparable estimation accuracy (Fig. 3E), leading to significantly smaller steady-state errors, as compared to AVA (Fig. 3A). Moreover, the controller blending of CA+AVA and CA+eAVA does not have a noticeable influence on the convergence rate of the parameter errors.

B. Experiment #2: Trajectory Tracking with an Unknown Payload or under Mass Parameter Variations

The second experiment evaluates the tracking performance of the proposed framework in the presence of different types of model uncertainties. The desired trajectory is $\boldsymbol{q}_{\mathrm{d}}(t) = \boldsymbol{q}_0 + \boldsymbol{q}_{\mathrm{dev}}(1 - \cos(\omega t))$ with $\boldsymbol{q}_0$ the initial configuration, $\boldsymbol{q}_{\mathrm{dev}} = [1, -1, -1, 1, 1, 1, -1]^T \frac{\pi}{12}\mathrm{rad}$, and $\omega = 1.57\,\frac{\mathrm{rad}}{\mathrm{s}}$. Similar to Experiment #1, initial position errors are intentionally assigned. Fig. 4 shows the results of the tracking case with the same payload used in Experiment #1. Note that CA will lead to violation of actuator constraints and cannot be started, since both a high feedback gain ($K_i = 20$) and large initial errors ($|\tilde{q}_i(t_0)| = 0.21\,\mathrm{rad}$) are applied. As seen in Fig. 4 (left), the proposed CA+eAVA with different a_i successfully prevents the performance degradation caused by the model mismatch, while preserving the advantageous low-gain behavior of AVA under large control errors. In comparison, CA+AVA delivers similar tracking performance only after the first round (i.e., $4\,\mathrm{s}$) of the periodic trajectory, and AVA shows the worst performance due to the lack of online model corrections. All approaches with CA can reduce the mass estimation errors by at least $80\,\%$ after finishing the trajectory (Fig. 4B). They feature small, steady-state prediction errors (Fig. 4E) mainly attributed to nonparametric uncertainties such as joint friction and measurement noise.

The results with mass parameter variations of all links are shown in Fig. 5. The initial estimates of the mass parameters

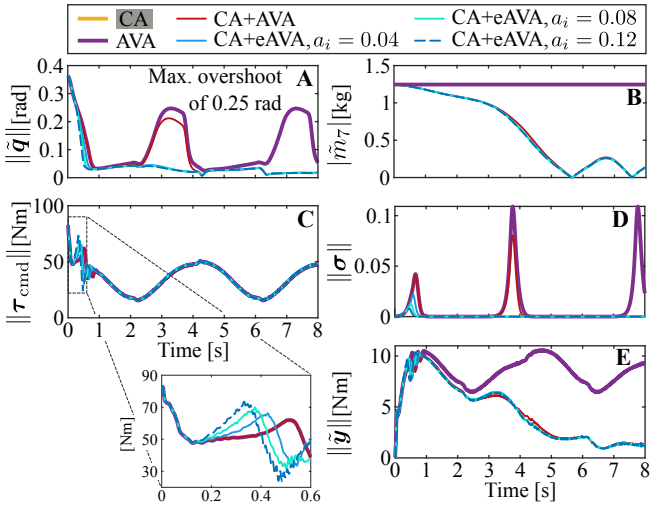

Fig. 4. Experiment #2a: Tracking case with the same payload at the end-effector as used in Exp. #1. The absolute initial position error on the joints 1, 2, and 4 is 0.21 rad each. CA cannot be started due to actuator constraints.

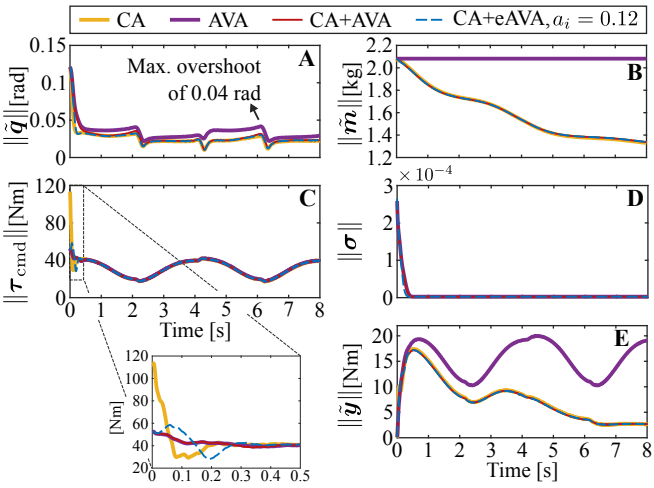

Fig. 5. Experiment #2b: Tracking case under mass parameter variations of all links. The term $\tilde{\boldsymbol{m}}$ denotes the estimation errors of all link masses. Their initial estimates are set to 50 % of the respective nominal values. The absolute initial position error on the joints 1, 2, and 4 is 0.07 rad each.

are set to 50 % of their nominal values, and the parameter adaptation is activated for all links. Except for the original AVA, all controllers achieve similar tracking performance (Fig. 5A) and comparable error convergence (Fig. 5B, 5E). Although CA can be executed due to the smaller initial position error ($|\tilde{q}_i(t_0)| = 0.07$ rad), it generates considerably larger commanded torques (Fig. 5C), of which the maximum Euclidean norm is around twice that with AVA applied. Note that the internal states do not grow during the transient (Fig. 5D, cf. Fig. 4D), since $|\tilde{q}_i| \leq \breve{q}_i = 0.07$ rad is always satisfied for $i = 1, \ldots, 7$. This exemplifies the practical usage of the eAVA tuning strategy introduced in Section III-C.

C. Experiment #3: Regulation under External Disturbances

The third experiment verifies that the proposed framework can generate compliant motions and effectively reduce parameter drift under external disturbances. Compared to the previous experiments, a larger γ is used to amplify the effects

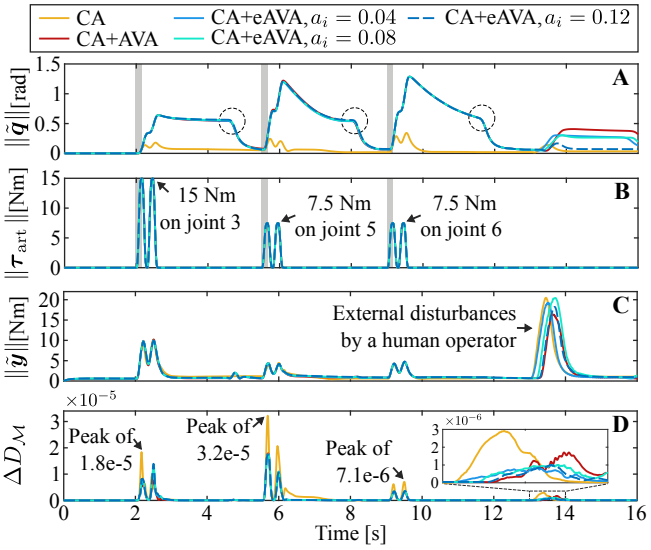

Fig. 6. Experiment #3: Regulation case under external disturbances. The term $\Delta D_{\mathcal{M}}$ denotes the computed parameter updates via (5), and $\boldsymbol{\tau}_{\mathrm{art}}$ the artificial external torques. No initial position and parameter errors are introduced in this case. For CA+AVA/eAVA, the *local-to-global* controller transitions caused by $\boldsymbol{\tau}_{\mathrm{art}}$ are highlighted by the shaded rectangles. The dashed circles mark the moments when E_i^* of the joints 3, 5, and 6 starts to increase, respectively, yielding the *global-to-local* controller transition.

of disturbances on parameter adaptation, while a smaller $K_{\mathrm{g},i}$ is chosen for more compliance. The metric (5) is utilized to compute the sum of parameter updates of all links at each time step, i.e., $\Delta D_{\mathcal{M}}(t_k) = \sum_{i=1}^{7} D_{\mathcal{M}}(\boldsymbol{\pi}_{i,t_{k-1}}, \boldsymbol{\pi}_{i,t_k})$. The results are shown in Fig. 6. To provide reproducible test conditions, artificial external torques are generated on the joints 3, 5, and 6 via additional motor commands (Fig. 6B). These impulse-like torques approximate the sudden impacts exerted on the robot due to collisions. Moreover, the robot is pushed by a human operator at the elbow joint; the resulting disturbance torques are shown in Fig. 6C. From Fig. 6A and the accompanying video, it can be observed that with CA+AVA/eAVA the robot behaves more compliantly under external disturbances, as compared to using CA only. Furthermore, due to the local-to-global controller transition, as highlighted by the shaded rectangles, AVA-based approaches feature less severe parameter drift (Fig. 6D). Note that the high-frequency, artificial external torques are considerably attenuated in the prediction error due to the low-pass filter (Fig. 6C); thus, they do not impede the local-to-global controller transition of CA+eAVA via the uncertainty measure. On the other hand, applying CA+eAVA with $a_i = 0.12$ results in less compliance under the low-frequency physical interaction with the human operator.

V. Conclusion and Discussion

This letter presented an adaptive control framework that incorporates: 1) the composite adaptive control scheme with the natural adaptation law to effectively handle model uncertainties, and 2) the AVA technique to smoothly modify feedback action according to both control errors and system uncertainties. An extended AVA was proposed involving an uncertainty measure in the variance adaptation, thereby allowing the proposed framework to anticipate significant modeling errors and prevent unnecessary performance degradation.

The global convergence and boundedness properties of the closed-loop system have been formally proved. The proposed framework was validated through experiments on a 7-DOF torque-controlled robot and comprehensively compared with several baseline schemes. As demonstrated by the experimental results, our framework can cope with both large modeling and control errors simultaneously, while it generally avoids extreme control commands and improves robustness against external disturbances. For future work, our approach can be extended to include nonparametric regression algorithms, similarly to semi-parametric learning [29], in order to counteract nonparametric uncertainties.

APPENDIX

The main results of [27] are recalled here to assist in the proof of Proposition 1.

Theorem 1: [27] Consider the interconnected system

$$\dot{\boldsymbol{x}}_1 = \boldsymbol{f}_1(\boldsymbol{x}_1, \boldsymbol{x}_2, \boldsymbol{u}_1) \tag{33a}$$

$$\dot{\boldsymbol{x}}_2 = \boldsymbol{f}_2(\boldsymbol{x}_1, \boldsymbol{x}_2, \boldsymbol{u}_2) \tag{33b}$$

where, for $i = 1, 2$, $\boldsymbol{x}_i \in \mathbb{R}^{n_i}$, $\boldsymbol{u}_i \in \mathbb{R}^{m_i}$, *and* $\boldsymbol{f}_i : \mathbb{R}^{n_1} \times \mathbb{R}^{n_2} \times \mathbb{R}^{m_i} \to \mathbb{R}^{n_i}$ *is locally Lipschitz. Assume that, for* $i = 1, 2$, *there exists an ISS-Lyapunov function* V_i *for the* $\boldsymbol{x}_i$*-subsystem such that the following holds:*

1) *there exist functions* $\phi_{i1}, \phi_{i2} \in \mathcal{K}_\infty$ *such that*

$$\phi_{i1}(\|\boldsymbol{x}_i\|) \leq V_i(\boldsymbol{x}_i) \leq \phi_{i2}(\|\boldsymbol{x}_i\|),\ \forall \boldsymbol{x}_i \in \mathbb{R}^{n_i}\ ;$$

2) *there exist functions* $\alpha_i \in \mathcal{K}_\infty$, $\chi_i, \rho_i \in \mathcal{K}$, *such that* $V_1(\boldsymbol{x}_1) \geq \max\{\chi_1(V_2(\boldsymbol{x}_2)), \rho_1(\|\boldsymbol{u}_1\|)\}$ *implies*

$$\frac{\partial V_1}{\partial \boldsymbol{x}_1} \boldsymbol{f}_1(\boldsymbol{x}_1, \boldsymbol{x}_2, \boldsymbol{u}_1) \leq -\alpha_1(V_1)\ ,$$

and $V_2(\boldsymbol{x}_2) \geq \max\{\chi_2(V_1(\boldsymbol{x}_1)), \rho_2(\|\boldsymbol{u}_2\|)\}$

$$\frac{\partial V_2}{\partial \boldsymbol{x}_2} \boldsymbol{f}_2(\boldsymbol{x}_1, \boldsymbol{x}_2, \boldsymbol{u}_2) \leq -\alpha_2(V_2)\ ;$$

3) $\chi_1 \circ \chi_2(r) < r,\ \forall r > 0$, *or* $\chi_2 \circ \chi_1(r) < r,\ \forall r > 0$.

Then, the system (33) *is ISS with respect to the state* $[\boldsymbol{x}_1^T, \boldsymbol{x}_2^T]^T \in \mathbb{R}^{n_1+n_2}$ *and the input* $[\boldsymbol{u}_1^T, \boldsymbol{u}_2^T]^T \in \mathbb{R}^{m_1+m_2}$.

REFERENCES

[1] J.-J. E. Slotine and W. Li, "On the adaptive control of robot manipulators," *The International Journal of Robotics Research*, vol. 6, no. 3, pp. 49–59, 1987.

[2] R. Middleton and G. Goodwin, "Adaptive computed torque control for rigid link manipulations," *Systems & Control Letters*, vol. 10, no. 1, pp. 9–16, 1988.

[3] J. J. E. Slotine and W. Li, "Composite adaptive control of robot manipulators," *Automatica*, vol. 25, no. 4, pp. 509–519, 1989.

[4] T. Lee, J. Kwon, and F. C. Park, "A natural adaptive control law for robot manipulators," *IEEE International Conference on Intelligent Robots and Systems*, pp. 8628–8635, 2018.

[5] S. Traversaro, S. Brossette, A. Escande, and F. Nori, "Identification of fully physical consistent inertial parameters using optimization on manifolds," in *IEEE/RSJ International Conference on Intelligent Robots and Systems*, 2016, pp. 5446–5451.

[6] P. M. Wensing, S. Kim, and J.-J. E. Slotine, "Linear matrix inequalities for physically consistent inertial parameter identification: A statistical perspective on the mass distribution," *IEEE Robotics and Automation Letters*, vol. 3, no. 1, pp. 60–67, Jan. 2018.

[7] G. Garofalo, X. Wu, and C. Ott, "Adaptive passivity-based multi-task tracking control for robotic manipulators," *IEEE Robotics and Automation Letters*, vol. 6, no. 4, pp. 7129–7136, Oct. 2021.

[8] M. Spong, "On the robust control of robot manipulators," *IEEE Transactions on Automatic Control*, vol. 37, no. 11, pp. 1782–1786, 1992.

[9] M. Krstić, I. Kanellakopoulos, and P. V. Kokotović, *Nonlinear and Adaptive Control Design*. New York: Wiley, 1995.

[10] N. T. Alberto, M. Mistry, and F. Stulp, "Computed torque control with variable gains through Gaussian process regression," in *IEEE-RAS International Conference on Humanoid Robots*, 2014, pp. 212–217.

[11] T. Beckers, D. Kulic, and S. Hirche, "Stable Gaussian process based tracking control of Euler-Lagrange systems," *Automatica*, vol. 103, pp. 390–397, 2019.

[12] M. K. Helwa, A. Heins, and A. P. Schoellig, "Provably robust learning-based approach for high-accuracy tracking control of Lagrangian systems," *IEEE Robotics and Automation Letters*, vol. 4, no. 2, pp. 1587–1594, Apr. 2019.

[13] M. Jin, J. Lee, and N. G. Tsagarakis, "Model-free robust adaptive control of humanoid robots with flexible joints," *IEEE Transactions on Industrial Electronics*, vol. 64, no. 2, pp. 1706–1715, Feb. 2017.

[14] J. Lee, H. Dallali, M. Jin, D. G. Caldwell, and N. G. Tsagarakis, "Robust and adaptive dynamic controller for fully-actuated robots in operational space under uncertainties," *Autonomous Robots*, vol. 43, no. 4, pp. 1023–1040, Apr. 2019.

[15] J. Lee, P. H. Chang, and M. Jin, "An adaptive gain dynamics for time delay control improves accuracy and robustness to significant payload changes for robots," *IEEE Transactions on Industrial Electronics*, vol. 67, no. 4, pp. 3076–3085, 2020.

[16] A. Dietrich, X. Wu, K. Bussmann, M. Harder, M. Iskandar, J. Englsberger, C. Ott, and A. Albu-Schäffer, "Practical consequences of inertia shaping for interaction and tracking in robot control," *Control Engineering Practice*, vol. 114, p. 104875, 2021.

[17] M. Llama, R. Kelly, and V. Santibanez, "Stable computed-torque control of robot manipulators via fuzzy self-tuning," *IEEE Transactions on Systems, Man, and Cybernetics, Part B (Cybernetics)*, vol. 30, no. 1, pp. 143–150, 2000.

[18] J. Armendariz, V. Parra-Vega, R. García-Rodríguez, and S. Hirai, "Dynamic self-tuning PD control for tracking of robot manipulators," in *IEEE Conference on Decision and Control*, 2012, pp. 1172–1179.

[19] G. Garofalo, "Global asymptotic stabilization with smooth high-gain/low-gain transitions: AVA - Adaptive variance algorithm," *IFAC-PapersOnLine*, vol. 52, no. 16, pp. 25–30, 2019.

[20] G. Garofalo and G. Mesesan, "A smooth uniting controller for robotic manipulators: An extension of the adaptive variance algorithm (AVA)," in *American Control Conference*, 2020, pp. 3224–3229.

[21] J. J. E. Slotine and W. Li, *Applied Nonlinear Control*. New Jersey: Prentice Hall, 1991.

[22] F. Ghorbel, B. Srinivasan, and M. W. Spong, "On the uniform boundedness of the inertia matrix of serial robot manipulators," *Journal of Robotic Systems*, vol. 15, no. 1, pp. 17–28, 1998.

[23] R. Gunawardana and F. Ghorbel, "On the uniform boundedness of the Coriolis/centrifugal terms in the robot equations of motion," *International Journal of Robotics and Automation*, vol. 14, no. 52, pp. 45–53, 1999.

[24] R. P. Paul, *Robot Manipulators: Mathematics, Programming, and Control*. Cambridge: MIT Press, 1981.

[25] T. Lee, P. M. Wensing, and F. C. Park, "Geometric robot dynamic identification: A convex programming approach," *IEEE Transactions on Robotics*, vol. 36, no. 2, pp. 348–365, 2020.

[26] A. Loria, "Observers are unnecessary for output-feedback control of Lagrangian systems," *IEEE Transactions on Automatic Control*, vol. 61, no. 4, pp. 905–920, 2016.

[27] Z.-P. Jiang, I. M. Mareels, and Y. Wang, "A Lyapunov formulation of the nonlinear small-gain theorem for interconnected ISS systems," *Automatica*, vol. 32, no. 8, pp. 1211–1215, 1996.

[28] G. Garofalo, C. Ott, and A. Albu-Schäffer, "On the closed form computation of the dynamic matrices and their differentiations," *IEEE/RSJ International Conference on Intelligent Robots and Systems*, pp. 2364–2359, 2013.

[29] J. Smith and M. Mistry, "Online simultaneous semi-parametric dynamics model learning," *IEEE Robotics and Automation Letters*, vol. 5, no. 2, pp. 2039–2046, 2020.